cmgh
CELLULAR AND MOLECULAR GASTROENTEROLOGY AND HEPATOLOGY

ORIGINAL RESEARCH

CD36 Deficiency Impairs the Small Intestinal Barrier and Induces Subclinical Inflammation in Mice

Vincenza Cifarelli,[1] Stoyan Ivanov,[2] Yan Xie,[3] Ni-Huiping Son,[5] Brian T. Saunders,[2] Terri A. Pietka,[1] Trevor M. Shew,[1] Jun Yoshino,[1] Sinju Sundaresan,[1] Nicholas O. Davidson,[3] Ira J. Goldberg,[5] Andrew E. Gelman,[4] Bernd H. Zinselmeyer,[2] Gwendalyn J. Randolph,[2] and Nada A. Abumrad[1]

[1]Department of Medicine, Center for Human Nutrition, [2]Department of Pathology and Immunology, [3]Department of Medicine, Division of Gastroenterology, and [4]Department of Surgery, Washington University School of Medicine, St Louis, Missouri; and [5]Department of Medicine, Division of Endocrinology, Diabetes and Metabolism, New York University Langone Medical Center, New York, New York

SUMMARY

This study documents that CD36 is important for intestinal homeostasis. CD36 deletion associates in the gut with altered extracellular matrix, neutrophil infiltration, and defective epithelial barrier. Systemically, the deletion results in subclinical inflammation with depletion of the Ly6C^{low} anti-inflammatory monocytes. Specific loss of endothelial cell CD36 recapitulates most intestinal phenotypes of germline CD36KO mice.

BACKGROUND & AIMS: CD36 has immunometabolic actions and is abundant in the small intestine on epithelial, endothelial, and immune cells. We examined the role of CD36 in gut homeostasis by using mice null for CD36 (CD36KO) and with CD36 deletion specific to enterocytes (Ent-CD36KO) or endothelial cells (EC-CD36KO).

METHODS: Intestinal morphology was evaluated by using immunohistochemistry and electron microscopy. Intestinal inflammation was determined from neutrophil infiltration and expression of cytokines, toll-like receptors, and cyclooxygenase-2. Barrier integrity was assessed from circulating lipopolysaccharide and dextran administered intragastrically. Epithelial permeability to luminal dextran was visualized by using two-photon microscopy.

RESULTS: The small intestines of CD36KO mice fed a chow diet showed several abnormalities including extracellular matrix accumulation with increased expression of extracellular matrix proteins, evidence of neutrophil infiltration, inflammation, and compromised barrier function. Electron microscopy showed shortened desmosomes with decreased desmocollin 2 expression. Systemically, leukocytosis and neutrophilia were present together with 80% reduction of anti-inflammatory Ly6C^{low} monocytes. Bone marrow transplants supported the primary contribution of non-hematopoietic cells to the inflammatory phenotype. Specific deletion of endothelial but not of enterocyte CD36 reproduced many of the gut phenotypes of germline CD36KO mice including fibronectin deposition, increased interleukin 6, neutrophil infiltration, desmosome shortening, and impaired epithelial barrier function.

CONCLUSIONS: CD36 loss results in chronic neutrophil infiltration of the gut, impairs barrier integrity, and systemically causes subclinical inflammation. Endothelial cell CD36 deletion reproduces the major intestinal phenotypes. The findings suggest an important role of the endothelium in etiology of gut inflammation and loss of epithelial barrier integrity. *(Cell Mol Gastroenterol Hepatol 2017;3:82–98; http://dx.doi.org/10.1016/j.jcmgh.2016.09.001)*

Keywords: Neutrophils; Endothelium; Fibronectin; Collagen.

The scavenger receptor CD36 mediates intracellular signaling in response to its ligands in a cell-type and context-dependent manner.[1] In the small intestine, CD36 is abundantly expressed on enterocytes, endothelial cells, and immune cells. CD36 present on the apical membrane of enterocytes recognizes dietary long-chain fatty acids and cholesterol and is important for chylomicron production.[2] CD36 null (CD36KO) mice have delayed intestinal lipid absorption, resulting in more fat reaching the distal gut, and produce smaller chylomicrons that are slowly cleared from the circulation.[3,4] The absorptive intestinal epithelium functions as a tight barrier limiting entry of pathogens and related toxins such as lipopolysaccharides.[5] Recruitment of immune cell to the gut elicits the acute inflammation necessary for host defense and later contributes to inflammation resolution and tissue healing.[6,7] CD36's role in gut immunity is unknown, but on monocytes/macrophages CD36 functions in recognizing pathogen-associated and

Abbreviations used in this paper: **COX-2, cyclooxygenase 2; ECM, extracellular matrix; FITC, fluorescein isothiocyanate; IL, interleukin; MPO, myeloperoxidase; PBS, phosphate-buffered saline; qRT-PCR, quantitative reverse transcription-polymerase chain reaction; SEM, standard error of the mean; α-SMA, smooth muscle actin alpha; TLR, toll-like receptor; TNF, tumor necrosis factor; TUNEL, deoxyuride-5'-triphosphate biotin nick end labeling.**

Most current article

2352-345X
http://dx.doi.org/10.1016/j.jcmgh.2016.09.001

danger-associated molecular pattern molecules that can initiate and sustain inflammatory responses.[8,9] CD36 also participates in resolution of inflammation by inducing polarization of macrophages to the anti-inflammatory M2 phenotype important for phagocytic clearance of apoptotic neutrophils[10] and tissue healing.[11,12] On endothelial cells, CD36 functions as a receptor for extracellular matrix (ECM) components such as thrombospondin 1 and collagen and acts as a signaling platform for several integrins.[13,14] Interaction of immune cells with the ECM is crucial to their activation and survival.[15,16] ECM dysregulation promotes tissue inflammation and might contribute to etiology of inflammatory bowel disease.[17]

The range of functions for intestinal CD36 (absorption, immunity, ECM) suggests it could play an important role in intestinal homeostasis, but this remains unexplored. In the present study, we examined the impact of CD36 deletion on intestinal barrier integrity and inflammation in mice fed a chow diet under basal conditions and after administration of a fat bolus. We show that germline CD36 deletion results in abnormal ECM remodeling, defective epithelial barrier, and neutrophil infiltration in the proximal intestine. Systemically, the deletion associates with endotoxemia and subclinical inflammation. Specific deletion of endothelial CD36 also results in a leaky epithelium and gut neutrophil infiltration, supporting a primary role in eliciting the gut abnormalities of the germline CD36KO mouse.

Materials and Methods

Animals

All studies followed guidelines of the animal ethics committee of Washington University School of Medicine (St Louis, MO). CD36-null (CD36KO), enterocyte null (Ent-CD36KO), endothelial null (EC-CD36KO), and wild-type (WT) mice, all on the C57BL/6 background, were housed in a facility with a 12-hour light-dark cycle and fed chow ad libitum (Purina, St Louis, MO) or when indicated fasted for 12 hours with ad libitum access to water. CD36 floxed (Fl/Fl) mice were generated by using a plasmid with LoxP sites flanking CD36 exons 2 and 3. After electroporation, selection, and screening, properly targeted ES clones were injected into blastocyst for generation of chimeric mice. Mice carrying the CD36 floxed allele were crossed with C57BL6 mice expressing Cre recombinase driven by the villin promoter (B6.Cg-Tg(Vil-cre)997Gum/J, stock number 021504; Jackson Laboratory, Bar Harbor, ME) to disrupt CD36 expression in enterocytes (Ent-CD36KO).

To delete endothelial CD36 (EC-CD36KO), CD36 floxed mice were crossed to C57BL6 mice expressing Cre driven by the Tie2 promoter. To avoid germline transmission, breeding involved Cre+ males with Cre– females. Genotypes were confirmed by polymerase chain reaction and immunohistochemistry. Endothelial cells were isolated from lungs of Fl/Fl and EC-CD36KO mice by using CD146 MicroBeads (Miltenyi Biotech, Cambridge, MA; cat. #130-092-007), and RNA from ~500,000 $CD146^+$ cells was used to measure CD31 and CD36 mRNA levels by quantitative reverse transcription-polymerase chain reaction (qRT-PCR).

For the bone marrow chimera experiments, B6.SJL-$Ptprc^aPep3^b$/BoyJ mice (Jackson Laboratories) with the CD45.1 allelic version of the CD45 leukocyte common antigen were irradiated (1100 rad by using a cesium source) and injected retro-orbitally with the appropriate WT or CD36KO bone marrow suspension (2×10^6 cells) as previously described.[18] Blood and intestines were collected 8 weeks later for flow cytometry and immunohistochemistry.

Intestine Permeability and Endotoxin Measurement

Fluorescein isothiocyanate (FITC)–conjugated dextran (4 kDa) (Sigma-Aldrich, St Louis, MO) was intragastrically administered to mice (n = 6/genotype) sedated initially with 4%–5% isoflurane and maintained with 1%–2% isofluorane. Blood was collected retro-orbitally at 0, 2, 4, and 6 hours, and level of FITC-dextran was measured at excitation 485/20 and 528/20 emission (Synergy HT; BioTek Instruments Inc, Winooski, VT). One week later, the experiment was repeated by using the same mice groups, but a bolus of triolein (4.5 μL/g body weight) was administered intragastrically 30 minutes before the FITC-dextran. For endotoxin determinations, sera were diluted 1:20, heated (70°C, 15 minutes), and assayed by using the limulus amebocyte lysate chromogenic endotoxin quantification (Lonza Inc, Walkersville, MD).

Histology and Immunohistochemistry

Small intestines were gently washed in cold phosphate-buffered saline (PBS), opened longitudinally, fixed in 10% formalin, and paraffin embedded. Sections (5 μm) were deparaffinized, followed by antigen retrieval (99°C, 18 minutes) in a pressurized chamber (Biocare Medical, Concord, CA) and blocked (1 hour) in donkey serum (2%) (Jackson Laboratories) and bovine serum albumin (3%) (Sigma-Aldrich). Incubation with primary antibodies (Table 1) was performed overnight (4°C), followed by incubation with horseradish peroxidase (Jackson Immuno Research Laboratories, West Grove, PA) or fluorescently labeled secondary antibodies (1 hour) (Alexa Fluor; BD Bioscience, San Jose, CA). For bone marrow staining, mouse femurs were fixed with 4%

Table 1. List of Antibodies, Source, and Dilution Used

Antigen	Host	Source	Dilution
MPO	Rabbit	Abcam	1:200
TLR2	Mouse	R&D Systems	1:100
Collagen 1α	Rabbit	Abcam	1:250
Fibronectin	Rabbit	Abcam	1:250
α-SMA	Rabbit	Sigma-Aldrich	1:500
CD36	Goat	R&D Systems	1:100
CD31	Mouse	BD Bioscience	1:500

paraformaldehyde in PBS at 4°C for 2 days, decalcified in 20% ethylenediamine tetraacetic acid (4°C, 2–4 weeks), and paraffin embedded. Longitudinal 5-μm sections were stained for myeloperoxidase (MPO) (Thermo Fisher Scientific, Waltham, MA; dilution 1:200) and deoxyride-5'-triphosphate biotin nick end labeling (TUNEL) (Roche Life Science, Indianapolis, IN), and images were taken by using a Nikon (Tokyo, Japan) Eclipse TE2000-U microscope.

Intravital Two-Photon Microscopy

Gut imaging was as previously described.[19] Mice anesthetized by intraperitoneal injection of ketamine (50 mg/kg) and xylazine (10 mg/kg) were given halved doses (25 mg/kg and 5 mg/kg) every hour. A small vertical incision in the shaved mouse abdomen exteriorized the proximal jejunum (~6 cm), which was maintained moist with PBS irrigation. Dextran (10 kDa) conjugated to fluorescein (Thermo Fisher Scientific; cat. #D1820) was injected into the lumen (1 μg/100 μL PBS) and DyLight 594–conjugated tomato lectin (Vector Laboratories Inc, Burlingame, CA) retro-orbitally 10 minutes before imaging. The exteriorized intestine was irrigated with 0.5% scopolamine in PBS to dampen peristaltic movements. To image from the luminal surface, a small longitudinal incision was made avoiding large blood vessels, and images were collected for ~2 hours by using a customized Leica SP8 2-photon microscope (Brähler et al, 2016) equipped with ×25/0.95 NA water-dipping objective and Mai Tai HP DeepSee Laser (Spectra-Physics, Newport Corporation, Santa Clara, CA) tuned to 900 nm. Fluorescence emission was separated by 3 high-efficiency dichroic mirrors cutting at 458, 495, and 560 nm (Semrock Inc, Rochester, NY) and directed to 4 supersensitive external detectors. Three-dimensional stacks consisting of between 21 and 31 planes (2.5 μm step size) were captured every 30 seconds. During imaging the mice body temperature was maintained at 37°C by using a customized heatable box (Life Imaging Services GmbH, Basel, Switzerland). The leakage is expressed as fold change of FITC-dextran fluorescence measured inside the villus versus FITC-dextran fluorescence measured between epithelial cells in 5 random villi/mouse.

Transmission Electron Microscopy

Small intestines (n = 4/genotype) were collected, washed with cold PBS, opened longitudinally and fixed (1 hour, room temperature) with 2% paraformaldehyde/2.5% glutaraldehyde (Polysciences Inc, Warrington, PA) in 100 mmol/L cacodylate buffer, pH 7.2. Samples were washed in cacodylate, postfixed (1 hour) in 1% osmium tetroxide (Polysciences Inc), rinsed extensively in dH_2O, stained (1 hour) with 1% aqueous uranyl acetate (Ted Pella Inc, Redding, CA), and rinsed before dehydration in graded ethanol and embedding in Eponate 12 resin (Ted Pella). Sections of 95 nm were cut with a Leica Ultracut UCT ultramicrotome (Leica Microsystem Inc, Bannobuckburn, IL), stained with uranyl acetate and lead citrate, and viewed on a JEOL 1200 EX transmission electron microscope (JEOL USA Inc, Peabody, MA) with an AMT 8 megapixel digital camera (Advanced Microscopy Techniques, Woburn, MA).

Table 2. List of Primer Sequences

Gene	Forward	Reverse
Ncf-1	CTGGAGGGCAGAGACAATCC	AGGGATAGGAGCCGTCTAGG
Ncf-2	TAAACTGAGCTACCGGCGTC	CTGGCGTCTGAGTTTTCCCT
Ncf-4	AAGTGAGAGGTGAACTCGGC	AAGCTGCTCAAAGTCGCTCT
s100a8	GGAAATCACCATGCCCTCTA	GCTACTCCTTGTGGCTGTCTTT
S100a9	ACACCCTGAGCAAGAAGGAA	CCATCAGCATCATACACTCCTC
CD31	TCACCAAGAGAACGGAA	TTACTGCTTTCGGTGGG
CD36	GATGACGTGGCAAAGAACAG	CAGTGA AGGCTCAAAGATGG
Desmocollin 2	CTCTGGCTAGTTGCTGGTACT	GTGGGAAGGGACCCAATGAA
IL6	AGCCAGAGTCCTTCAGAGAGAT	GCACTAGGTTTGCCGAGTAGAT
IL1β	GTGTGTGACGTTCCCATTAGAC	GTCGTTGCTTGGTTCTCCTT
COX-2	CTCACGGAACTCAGCACT	TAGAATCCAGTCCGGGTACAGT
TNF-α	GATCGGTCCCCAAAGG	CACTTGGTGGTTTGCT
IL10	GGCGCTGTCATCGATTTCTCCCC	AGCTCTGTCTAGGTCCTGGAGTCC
IL22	GCTCAGCTCCTGTCACATCA	TCCCCAATCGCCTTGATCTC
TLR4	ATGGCATGGCTTACAC	GAGGCCAATTTTGTCT
Collagen 1α	CGATGGATTCCCGTTCGAGT	CGATCTCGTTGGATCCCTGG
Fibronectin	GCCACCATTACTGGTCTGGA	GGAAGGGTAACCAGTTGGGG
α-SMA	GTCCCAGACATCAGGGAGTAA	TCGGATACTTCAGCGTCAGGA
JNK 1	CAAGCACCTTCACTCTGCTG	GTTCTCCTTGTAGCCCATGC
JNK 2	TGGCGGACTCAACTTTCAC	AGTTCACGGTAGGCTCTCTTTG
36B4	GCAGACAACGTGGGCTCCAAGCAGAT	GGTCCTCCTTGGTGAACACGAAGCCC

A

Geneset name	Z score	*P* value
KEGG_FOCAL_ADHESION	7.65	2.00E-14
KEGG_LEUKOCYTE_TRANSENDOTHELIAL_MIGRATION	6.13	8.99E-10
KEGG_ECM_RECEPTOR_INTERACTION	5.73	9.85E-09
KEGG_ETHER_LIPID_METABOLISM	5.57	2.54E-08
KEGG_VASCULAR_SMOOTH_MUSCLE_CONTRACTION	5.18	2.18E-07
KEGG_ALPHA_LINOLENIC_ACID_METABOLISM	5.15	2.66E-07
KEGG_LINOLEIC_ACID_METABOLISM	4.97	6.61E-07
KEGG_SULFUR_METABOLISM	4.56	5.19E-06
KEGG_GLYCEROLIPID_METABOLISM	4.53	5.96E-06

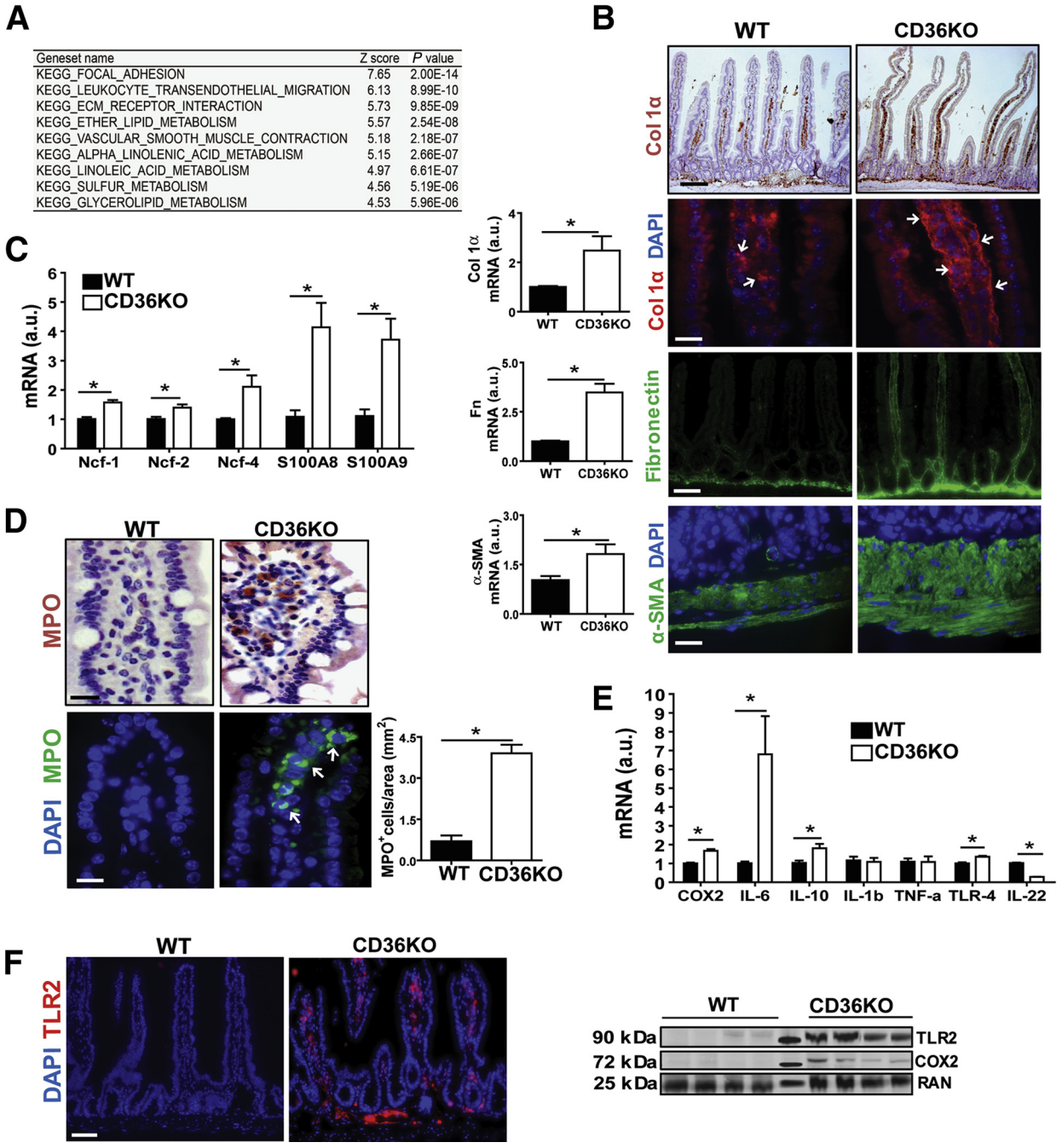

Figure 1. CD36 deletion causes remodeling of ECM proteins and immune cell infiltration in the small intestine. (*A*) Microarray analysis on proximal intestines showing the 9 most upregulated pathways in CD36KO mice as compared with controls, including those related to leukocyte transendothelial migration and ECM. (*B*) Altered ECM remodeling in intestines of CD36KO mice; qRT-PCR showing increased expression of ECM proteins: collagen 1α ($P = .01$), fibronectin ($P = .0003$), and α-SMA ($P = .04$) (n = 6/genotype; typical of 3 experiments). Immunostaining of collagen 1α, fibronectin, and α-SMA was also increased (n = 4/genotype; representative of 2 experiments). (*C* and *D*) Neutrophil infiltration of CD36KO intestines. (*C*) Increased expression of neutrophil cytoplasmic protein (Ncf)-1 ($P = .04$), Ncf-2 ($P = .02$), Ncf-4 ($P = .03$), S100A8 ($P = .007$), and S100A9 ($P = .01$) in CD36KO mice as compared with WT controls (n = 6/genotype; representative of 3 experiments) and (*D*) MPO immunohistochemical (*top panels*) and fluorescent (*bottom panels*) staining. Graph shows quantification of immunofluorescence ($P = .01$) (n = 4/genotype; representative of 2 experiments). (*E* and *F*) Altered expression of inflammatory mediators in CD36KO intestine: (*E*) COX-2 ($P = .0006$), IL6 ($P = .03$), IL10 ($P = .028$), TLR4 ($P = .04$), IL22 ($P = .03$) (n = 6/genotype; representative of 3 experiments), and (*F*) TLR2 immunostaining (images representative of 2 experiments, n = 4/genotype). Immunoblots show levels of COX-2 and TLR2 measured in intestinal lysates; *middle lane*: molecular weight markers, 25, 72, and 90 kDa. Scale bars: 25 μm for (*B*), lower col1α, α-SMA, and (*D*) 100 μm for (*B*), upper col1α, fibronectin, and for (*F*). All bar graphs show means ± standard error of the mean (SEM). *$P < .05$ by 2-tailed Student *t* test.

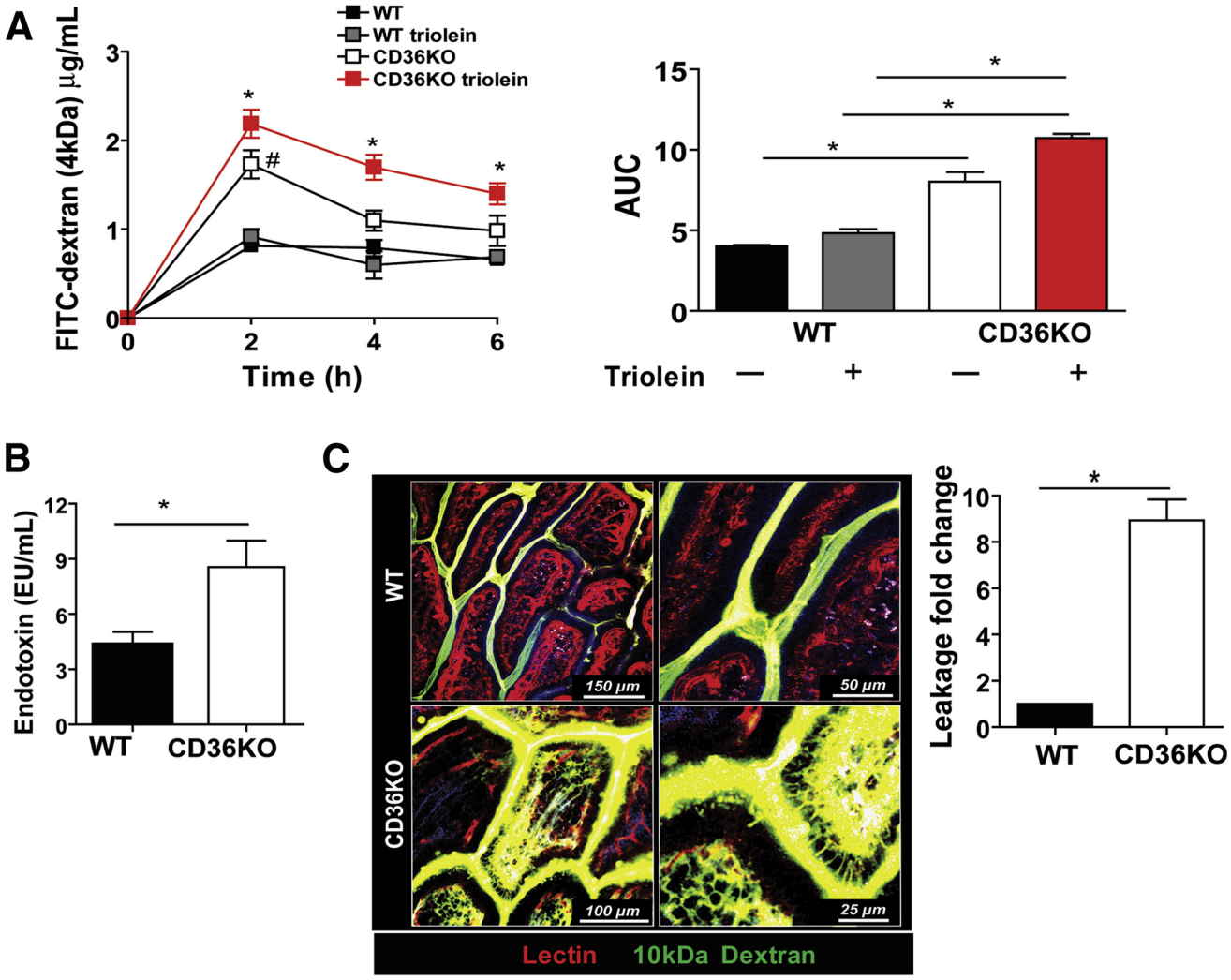
A
WT
WT triolein
CD36KO
CD36KO triolein
FITC-dextran (4kDa) μg/mL
Time (h)
AUC
WT
CD36KO
Triolein
B
Endotoxin (EU/mL)
WT
CD36KO
C
WT
CD36KO
150 μm
50 μm
100 μm
25 μm
Lectin 10kDa Dextran
Leakage fold change
D
WT
CD36KO
Length (nm)
E
Desmocollin 2 mRNA (A.U.)
F
WT
CD36KO
Occludin
β-actin
Occludin/β-actin

To measure desmosome length, AMT Image Capture Engine Software 602.524 (Advanced Microscopy Techniques) was used.

Flow Cytometry Analysis

Blood, bone marrow, and spleen samples were prepared as previously described.[20] Flow cytometry used an LSR II (Becton Dickinson, Franklin Lakes, NJ) and data analysis FlowJo software (Tree Star, Ashland, OR). Combinations of fluorochrome- or biotin-conjugated antibodies were used in staining: MHC class II I-A/I-E (clone M5/14.15.2), CD11b (clone M1/70), CD45 (clone 30-F11), CD45.1 (clone A20), CD45.2 (clone 104), CD115 (clone AFS98), Ly6C (clone HK1.4), Ly6G (clone 1A8), CD19 (clone 1D3), NK1.1 (clone PK 136), and Gr-1 (clone RBC-85).

RNA Extraction and Quantitative Reverse Transcription-Polymerase Chain Reaction

RNA extracted from the proximal small intestine (n = 6/genotype) by using TRIzol (Invitrogen, Carlsbad, CA) was subjected to cDNA reverse transcription and qRT-PCR (ABI Prim 7000 Sequence Detection System; Applied Biosystems, Foster City, CA) by using Power SYBR Green PCR Master Mix (Applied Biosystems) on a 7500 Fast Real Time PCR System (Applied Biosystems). Relative mRNA fold changes were determined by using standard δCt calculations (primers listed in Table 2).

Western Blotting

After electrophoresis (4%–12% acrylamide gradient), proteins were transferred to polyvinlyidene fluoride membranes (Merk Millipore Ltd, Cork, Ireland), blocked (Li-COR Biosciences, Lincoln, NE), and incubated overnight at 4°C with primary antibodies. Antibodies used were goat anti-mouse Ran (1:2000; Sigma-Aldrich), mouse anti-mouse TLR2 (1:1000; R&D Systems, Minneapolis, MN), cyclooxygenase-2 (COX-2) (1:1000; R&D Systems), β-actin (1:1000; Santa Cruz Technology, Santa Cruz, CA), occludin (1:1000; Thermo Fisher Scientific), JNK and p-JNK (1:1000; Cell Signaling Technology, Danvers, MA), and goat anti-mouse CD36 (R&D Systems; 1:2000). Incubation with infrared dye–labeled secondary antibodies was for 1 hour at room temperature, and protein signals were detected by using the Li-Cor Odyssey Infrared System (Li-COR Biosciences).

Microarray Study and Pathway Analysis

Proximal small intestine (upper one-third of the gut) was harvested and processed for RNA extraction and microarrays (Affymetrix GeneChip Mouse Expression Set 430 2.0 array; Affymetrix Bioscience, San Diego, CA). Parametric Analysis of Gene Set Enrichment (PAGE), as previously described,[21] used KEGG and C2: curated gene sets (http://www.broad.mit.edu/gsea/msigdb/msigdb_index.html). Z scores and P values were calculated for each set. All data were analyzed by the R statistical software package (http://www.bioconductor.org). P value $<.05$ was considered significant.

Results

CD36 Deletion Induces Extracellular Matrix Disruption, Neutrophil Infiltration, and Inflammation in the Proximal Small Intestine

CD36's function in lipid absorption is well-documented,[3,4,22] but little is known about its role in intestinal homeostasis. We first performed gene expression analysis of the proximal intestine, where CD36 is particularly abundant, by using CD36KO and WT control mice. The microarray analysis showed upregulation of pathways involved in ECM remodeling and leukocyte transendothelial migration (Figure 1*A*). Evidence of substantial ECM remodeling was observed in the intestine of CD36KO mice including increased mRNA for collagen 1α ($P = .01$), fibronectin ($P = .0003$), and alpha-smooth muscle actin (α-SMA) ($P = .04$) (Figure 1*B*). Immunohistochemistry documented increased collagen 1α deposition in the submucosa and on vessels within villi (Figure 1*B*) and fibronectin accumulation throughout villi and in the submucosa (Figure 1*B*). The

Figure 2. (***See previous page***). **Gut barrier permeability is impaired in CD36KO mice.** (*A*) Plasma level of FITC-dextran (4 kDa) measured at indicated times after its intragastric administration. A week later, same mice group received triolein bolus (4.5 μL/g body weight) 30 minutes before FITC-dextran. $^{\#}$WT versus CD36KO mice, *WT$_{\text{triolein}}$ versus CD36KO$_{\text{triolein}}$ mice. Levels in WT mice did not change with or without triolein bolus. Intestinal permeability was increased in all CD36KO mice at 2 hours ($P = .04$; $P_{\text{triolein}} = .032$) and remained increased at 4 hours ($P = .043$) and 6 hours ($P = .041$) in CD36KO mice given triolein. *Right panel* shows area under the curve (AUC) for CD36KO and CD36KO$_{\text{triolein}}$ mice was increased compared with appropriate controls ($P < .001$ and $P = .005$, respectively) and before as compared with after triolein challenge ($P < .001$). (*B*) Measurement of endotoxin in plasma of WT and CD36KO mice 4 hours after triolein challenge (n = 4/genotype), $P = .03$. (*C*) Two-photon microscopy optical sections showing leakage across the epithelium; fluorescein-dextran (10 kDa) (*green*) was administered intraluminally to intestines of anesthetized mice (n = 3/genotype) and DyLight 594–conjugated tomato lectin (*red*), a vascular marker, by retro-orbital injection 10 minutes before imaging from the luminal surface. Dextran leakage is observed in CD36KO mice but not in WT mice ($P < .01$). Quantification of leakage is expressed as fold change of FITC-dextran fluorescence inside the villus versus fluorescence between epithelial cells measured in 5 random villi/mouse. *Blue fluorescence,* 2-harmonic generation; *light purple fluorescence,* autofluorescence. Scale bars: WT, 150 and 50 μm; CD36KO, 100 and 25 μm. (*D*) Electron microscopy images showing shortened desmosomes in intestinal epithelium of CD36KO mice. Scale bar: 500 nm. Graph shows quantification of decrease in desmosome length (n = 20/genotype, $P = .001$). (*E*) Expression of desmosomal protein desmocollin 2 is decreased in intestines of CD36KO mice compared with controls ($P = .01$, n = 8/genotype). (*F*) Level of tight junctional protein occludin measured in intestinal lysates by immunoblotting and densitometry quantification of change in occludin/β-actin as compared with WT control ($P = .01$) (n = 4/genotype). Data are representative of 3 (*A–E*) and 2 (*F*) experiments. Bar graphs show means ± SEM.

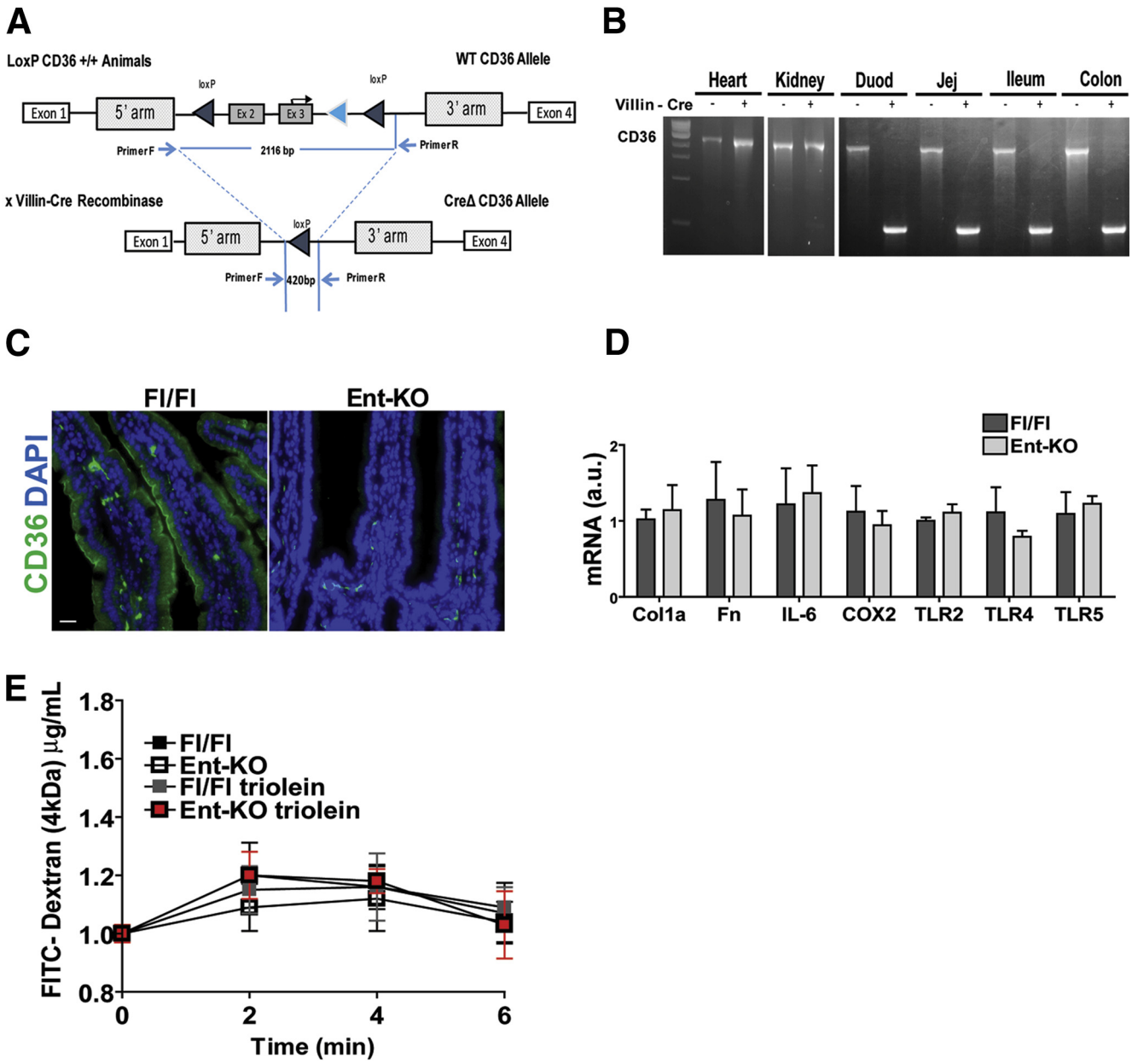

Figure 3. Deletion of CD36 in enterocytes does not alter gut permeability or associate with inflammation. (*A–C*) Generation and validation of a mouse with enterocyte specific CD36 deletion (Ent-KO). (*A*) Ent-KO CD36 mice were obtained by crossing CD36 floxed mice with mice carrying the villin-Cre recombinase. (*B*) PCR showing specific deletion of CD36 in the intestine but not in other tissues, Duod, duodenum; Jej, jejenum. (*C*) Immunofluorescence of intestinal sections from floxed controls (Fl/Fl) and Ent-KO mice showing absence of epithelial CD36 expression on enterocytes. Scale bar: 50 μm. (*D*) Intestines of Ent-KO mice do not display altered expression of collagen, fibronectin, and markers of inflammation. (*E*) Ent-KO mice did not show altered intestinal permeability measured by oral administration of FITC-dextran (4 kDa) as compared with floxed control mice. Values shown are means ± SEM. Data (*C–E*) are representative of 2 experiments, n = 6 per genotype.

muscularis appeared thickened as shown by the α-SMA staining (Figure 1*B*). Neutrophil infiltration in the CD36KO gut was evident from increased mRNA abundance of neutrophil cytosolic factors (Ncf)-1 ($P = .04$), Ncf-2 ($P = .02$), Ncf-4 ($P = .03$), and proteins S100A8 ($P = .007$) and S100A9 ($P = .01$) (Figure 1*C*) and from increased MPO staining (Figure 1*D*). Levels of mRNA for markers of inflammation and innate immunity were also increased including COX-2 ($P = .0006$), interleukin (IL) 6 ($P = .03$), IL10 ($P = .028$), and toll-like receptor (TLR) 4 ($P = .04$). Expression of IL22 was decreased ($P = .03$), whereas expression of IL1β and tumor necrosis factor (TNF)-α did not change (Figure 1*E*). Increased expression of COX-2 and TLR2 in intestine of CD36KO mice was confirmed by Western blot and immunofluorescence staining (Figure 1*F*). These data indicated that CD36 deletion results in altered ECM remodeling, inflammation, and neutrophil infiltration in the proximal small intestine.

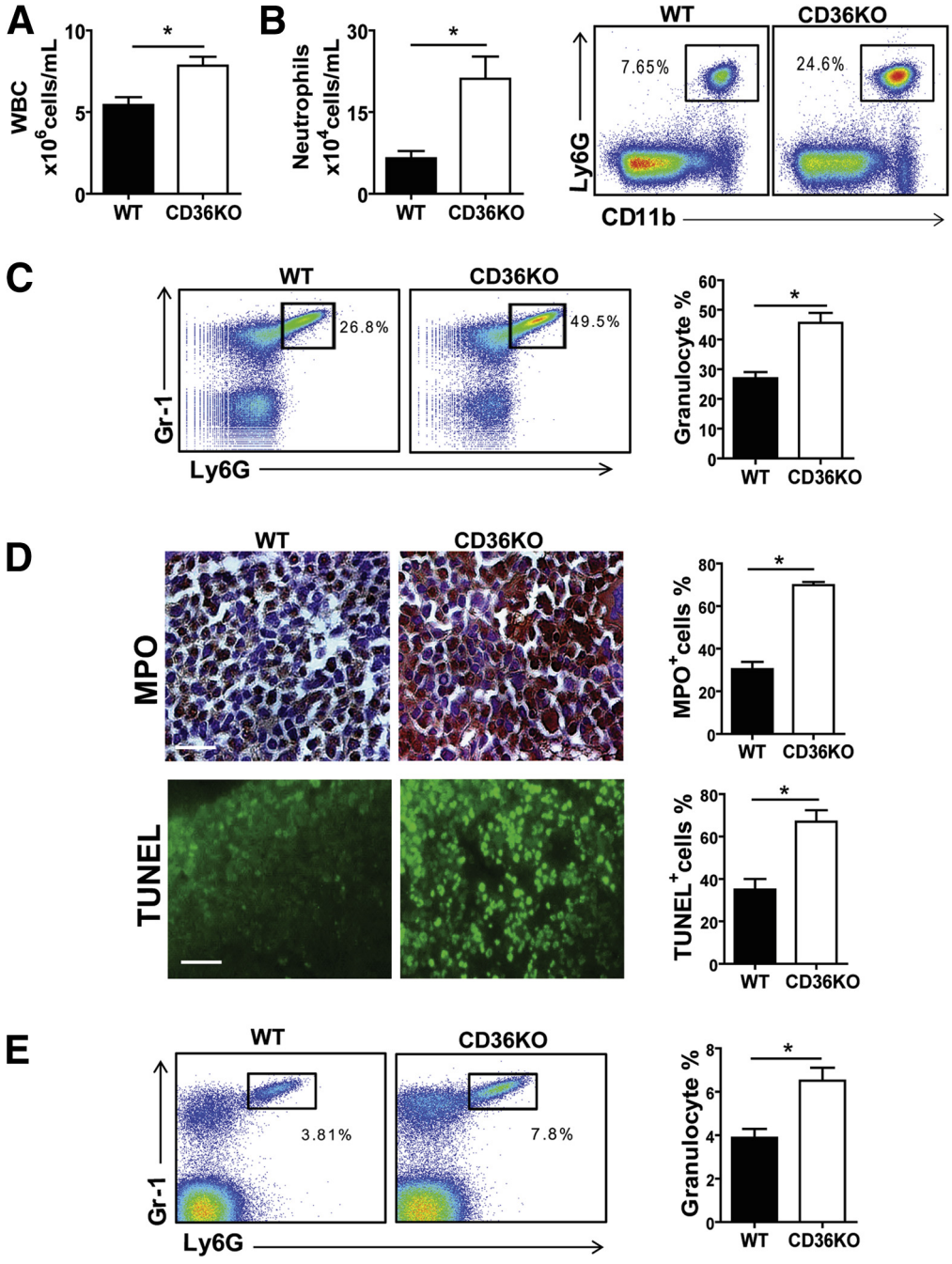

Figure 4. CD36 deletion induces systemic leukocytosis and neutrophilia. Peripheral blood was analyzed for white blood cells (WBC) and neutrophils by flow cytometry (n = 8/genotype). As compared with WT mice, CD36KO mice have (*A*) increased WBC count ($P = .007$) and (*B*) circulating neutrophils ($CD11b^+/Ly6G^+$) ($P = .004$). (*C*) Bone marrow neutrophil content ($Ly6G^+/Gr\text{-}1^+$) is increased in CD36KO mice ($P = .0015$) as compared with WT controls. (*D*) Representative images and quantification (based on 5 random fields/section) of bone marrow stained for MPO ($P = .01$) and TUNEL ($P = .002$) (n = 4/genotype). Scale bar: 2 μm. (*E*) Spleen neutrophil content ($Ly6G^+/Gr\text{-}1^+$) is increased in CD36KO as compared with WT mice ($P = .0067$) (n = 5/genotype). *A–E*, representative of 3 experiments. Graphs show mean ± SEM.

Increased Gut Permeability in CD36KO Mice

We next investigated whether the above changes associated with compromised barrier integrity by measuring plasma levels of intragastrically administered FITC-dextran (4 kDa) (n = 6 mice/genotype). To monitor the effect on permeability of intestinal fat absorption, which can induce transient inflammation,[23] a week later an intragastric fat challenge (4.5 μL triolein/kg body weight) was administered 30 minutes before the FITC-dextran to the same mice groups. As compared with WT controls, intestinal permeability was increased 2-fold in CD36KO mice at 2 hours, and the increase was similar when a triolein challenge was included ($P = .04$; $P_{triolein} = .032$) (Figure 2*A*). However, the increased leakage was sustained at 4 hours ($P = .043$) and 6 hours ($P = .041$) only in CD36KO mice given triolein (Figure 2*A*). Consistent with this, serum endotoxin was 2-fold higher ($P = .03$) in CD36KO mice after 4 hours of a triolein bolus (Figure 2*B*). Barrier permeability in the small intestine was evaluated further by using intravital two-photon microscopy, and a larger molecular weight fluorescein-dextran (10 kDa) was given intraluminally to anesthetized mice. CD36KO mice

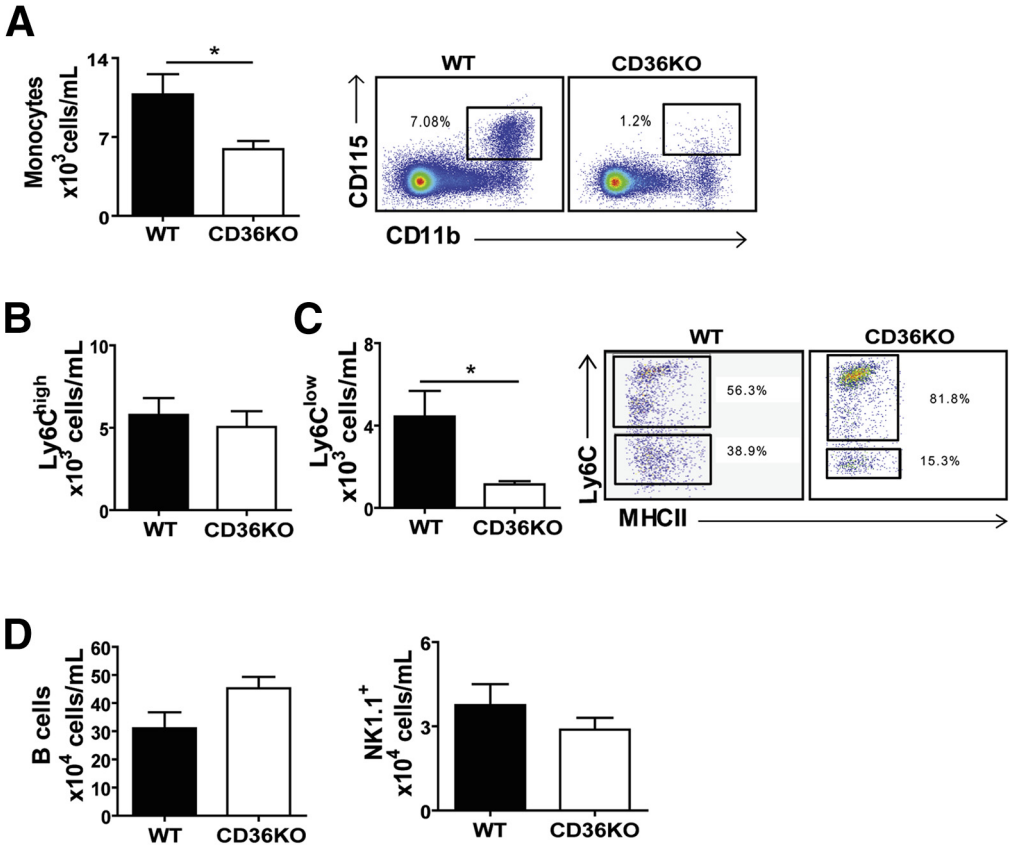

Figure 5. Circulating Ly6C^{low} monocytes are decreased in peripheral blood of CD36KO mice. As compared with WT controls, CD36KO mice show (*A*) lower monocyte number (CD115$^+$/CD11b$^+$) ($P = .05$), (*B*) similar number of Ly6C^{high} monocytes, and (*C*) lower number of Ly6C^{low} monocytes ($P = .01$). (*D*) B-cell (CD19$^+$) number trended higher, whereas that of NK/NK T cells (NK 1.1$^+$) was unchanged in CD36KO mice. (*A–D*) (n = 9/genotype) representative of 3 experiments. Bar graphs show means ± SEM. *$P < .05$ by 2-tailed Student *t* test.

showed significant dextran leakage across the epithelium, whereas no leakage was observed in control mice ($P < .01$) (Figure 2*C* and Supplementary Videos 1 and 2). The above data suggest that CD36 deletion, which results in gut neutrophil infiltration, also impairs integrity of the epithelial barrier.

Neutrophils can undergo transepithelial migration, impairing barrier function that may be transient or sustained.[7,24] The intercellular junction complexes (desmosomes, adherens, and tight junctions) provide barriers to neutrophil migration in paracellular spaces, and alterations of these structures affect barrier integrity. Electron microscopy on intestinal sections showed significant desmosome shortening in the epithelium of CD36KO mice (Figure 2*D*) ($P = .001$). Expression of the major desmosomal protein, desmocollin 2, was reduced in intestines of CD36KO mice as compared with controls ($P = .01$) (Figure 2*E*). Electron microscopy did not show obvious alteration of tight junction structures in the CD36KO epithelium, and gene expression of the major claudins (2, 3, 7, 12, 15) in the proximal intestine[25] was not altered on microarrays (data not shown). However, expression of occludin protein was reduced ($P < .01$) (Figure 2*F*) in CD36KO mice as compared with controls. These data suggest that altered desmosome structure and reduced expression of occludin and desmocollin 2 contribute to the impairment of epithelial barrier function observed in CD36KO mice.

Deletion of Enterocyte CD36 Does Not Alter Gut Permeability or Associate With Inflammation

Crosstalk between gut epithelial cells and immune cells is important for maintenance of tissue integrity and barrier function.[26,27] To determine whether loss of epithelial CD36 contributes to the abnormalities observed in CD36KO mice, we generated a mouse with enterocyte-specific CD36 deletion (Ent-CD36KO) (Figure 3*A–C*). The Ent-CD36KO mice showed no changes in expression of genes related to either the ECM or to inflammatory markers (Figure 3*D*) and displayed normal barrier integrity (data not shown). Thus, loss of enterocyte CD36 does not appear to play a primary role in driving the abnormal gut permeability or inflammation observed in germline CD36KO mice.

Presence of Leukocytosis and Neutrophilia in CD36KO Mice

We next asked whether the intestinal inflammation observed in CD36KO mice was associated with systemic changes in immune cells. A significant increase of white blood cell count ($P = .007$) and a 3-fold increase ($P = .004$) in circulating neutrophils (Ly6G$^+$/CD11b$^+$) were measured in CD36KO mice (Figure 4*A* and *B*). Neutrophils (Ly6G$^+$/Gr-1$^+$) were also increased in the bone marrow ($P = .0015$) (Figure 4*C*), and activation was suggested by

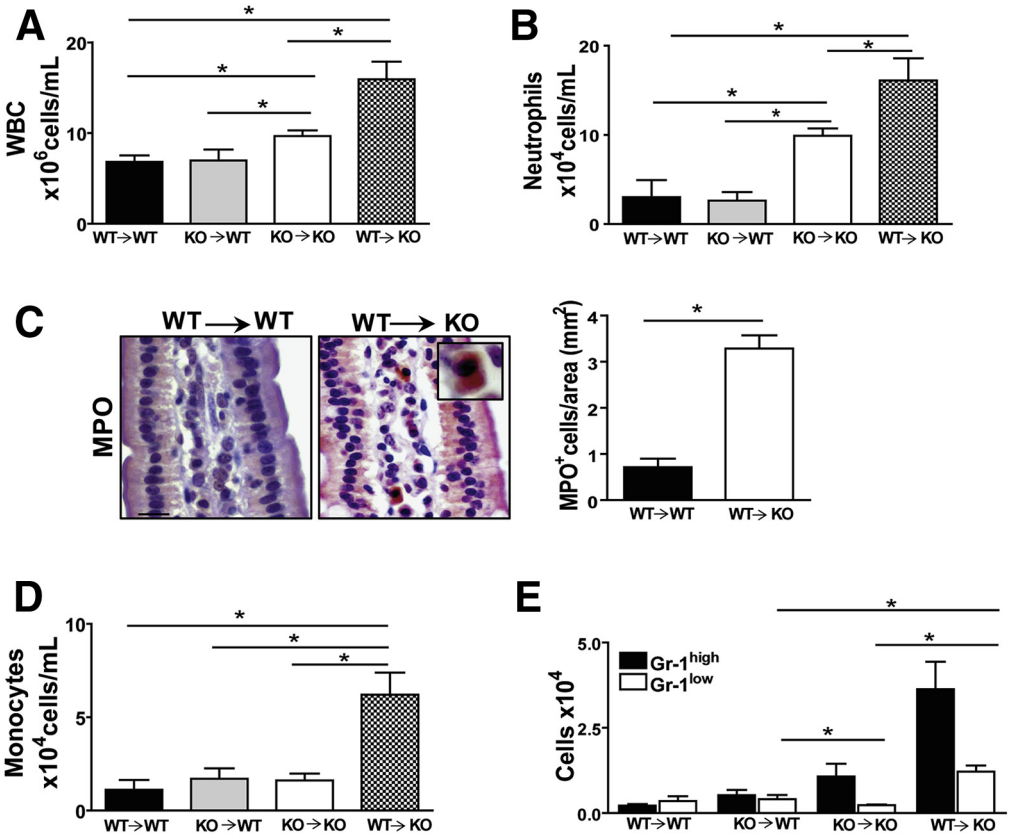

Figure 6. Bone marrow transplants support role of non-hematopoietic cells in the inflammation of CD36KO mice. (*A*) Chimeric mice lacking CD36 on non-hematopoietic cells (WT→KO) show highest level of leukocytosis as compared with control chimeric groups (WT→WT) ($P = .05$) and (KO→KO) ($P = .02$). WBC, white blood cells. (*B*) Neutrophil levels are also highest in WT→KO as compared with WT→WT ($P = .011$) and with KO→KO ($P = .05$) groups. (*C*) MPO staining showing neutrophil infiltration in small intestines of WT→KO group and quantification of MPO^+ cells in intestinal sections from 3 mice/group ($P = .01$). (*D*) Monocyte levels are highest in WT→KO as compared with WT→WT ($P = .018$) and KO→KO ($P = .01$) groups. (*E*) Levels of Gr-1^{low} are increased in WT→KO as compared with KO→KO ($P = .0001$) and KO→WT ($P = .009$) groups (n = 4/chimeric mice per group). (*A–E*) representative of 2 experiments. Graphs show data as means ± SEM.

intense MPO staining (Figure 4*D*) ($P < .01$). The increase in neutrophil numbers did not reflect lack of neutrophil apoptosis because TUNEL staining was increased in CD36KO bone marrow as compared with controls ($P < .01$) (Figure 4*D*); thus it appeared to be a likely consequence of defective phagocytosis by CD36 deficient macrophages.[10] Higher neutrophil levels ($Ly6G^+/Gr\text{-}1^+$) were also observed in spleens of CD36KO mice ($P = .0067$) (Figure 4*E*) and in the lungs (data not shown). The increase in circulating neutrophils (Figure 4*B–E*) and endotoxin levels (Figure 2*C*) suggested systemic subclinical inflammation in CD36KO mice.

Anti-inflammatory Ly6C^{low} Non-classic Monocyte Subset Is Markedly Reduced in CD36KO Mice

During tissue inflammation in addition to neutrophils, other immune cells, notably inflammatory monocytes,[28] are recruited from the bloodstream. Circulating monocytes ($CD115^+/CD11b^+$) were significantly lower in CD36KO mice as compared with control mice ($P = .05$) (Figure 5*A*). Two functionally distinct monocyte populations are present in mice and identified by expression of the lymphocyte antigen 6 complex (Ly6C); the Ly6C^{high} monocytes, referred to as inflammatory, are recruited to tissues during homeostasis[29] and in response to acute infection or injury.[30] The Ly6C^{low} monocytes, which can differentiate from the Ly6C^{high} [20], are referred to as anti-inflammatory. The Ly6C^{low} monocytes are termed *patrolling monocytes* on the basis of their chief function of surveying the luminal endothelium of blood vessels at steady state and in response to acute vascular inflammation.[20,30–33] The number of Ly6C^{high} monocytes was similar in WT and CD36KO mice, but there was marked reduction of Ly6C^{low} monocyte numbers ($P = .01$) (Figure 5*B* and *C*). We also investigated whether the numbers of other immune cell types were changed and found that B-cell number trended higher ($P = .09$) as previously reported,[34] whereas NK/NK T-cell number did not differ ($P = .2$) for WT and CD36KO mice (Figure 5*D*). The observation of reduced number of Ly6C^{low} monocytes (Figure 5*C*) together with the increase in the

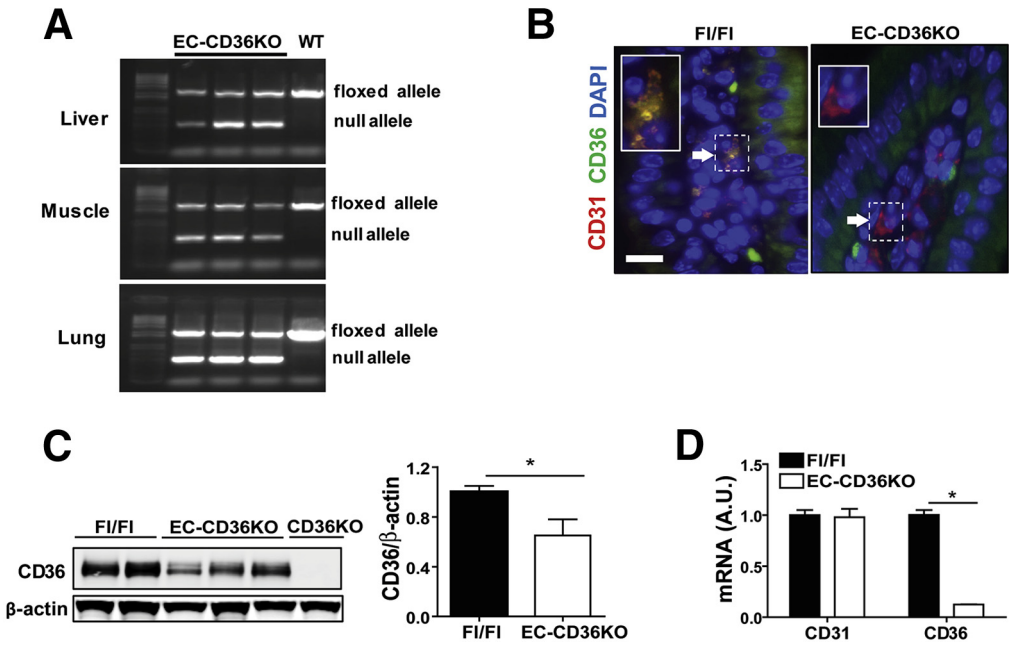

Figure 7. Generation and validation of a mouse with endothelial cell specific CD36 deletion. (*A*) A mouse with endothelial cell deletion of CD36 (EC-CD36KO) was generated by breeding floxed (Fl/Fl) CD36 mice with mice carrying the Tie2-Cre recombinase (Cre+ males with Cre– females). PCR of DNA isolated from liver, muscle, and lung tissues of EC-CD36KO and floxed mice showing presence of null allele in EC-CD36KO mice. (*B*) Staining of intestinal villi from EC-CD36KO and Fl/Fl control mice with CD31 (marker of endothelial cells) and CD36. *Insert*: Blowup of areas indicated by *white arrows* showing CD36 expression in $CD31^+$ cells in Fl/Fl but not in EC-CD36KO mice; scale bar: 30 μm. (*C*) CD36 protein levels in lysates from proximal intestines showing average 38% decrease in EC-CD36KO as compared with Fl/Fl mice (germline CD36KO mice are negative controls) ($P = .05$). (*D*) CD31 and CD36 mRNA expression in endothelial cells ($CD146^+$) isolated from lungs of Fl/Fl and EC-CD36KO mice (n = 3/genotype). CD36 mRNA levels are reduced in $CD146^+$ cells from EC-CD36KO mice as compared with Fl/Fl controls ($P < .01$), whereas CD31 mRNA levels are similar. Graphs show data as means ± SEM; n = 3/genotype.

transendothelial leukocyte migration pathway (Figure 1*A*) observed on microarrays suggested that the endothelium might be altered in CD36KO mice.

Non-hematopoietic Source of Inflammation in CD36KO Mice

To gain insight into the primary source of the systemic inflammation observed in CD36KO mice, bone marrow transplants were performed. The transfer of either CD36 sufficient or deficient bone marrow did not result in inflammation in WT recipient mice (WT→WT or KO→WT). However, inflammation was observed in CD36KO recipients regardless of the bone marrow source (WT→KO and KO→KO) (Figure 6*A*). Specifically, most significant leukocytosis was observed in the WT→KO group (Figure 6*A*), and a similar pattern was observed with neutrophil levels (Figure 6*B*). Furthermore, increased neutrophil infiltration was documented by MPO staining in small intestines of WT→KO mice (Figure 6*C*) compared with controls (WT→WT) ($P = .018$) (Figure 6*C*). Monocytes were higher only in the WT→KO group (Figure 6*D*) and reflected increases in both subsets Gr-1^{high} and Gr-1^{low} (Figure 6*E*). When compared with the KO→KO group, both Gr-1^{high} and Gr-1^{low} increased ($P = .08$ and $P = .0014$, respectively) in the WT→KO group, indicating that CD36 expression enhances levels of both proinflammatory and anti-inflammatory monocytes. There was no significant difference in T-cell and B-cell content among groups (data not shown). Overall, these data suggest that lack of CD36 on non-hematopoietic cells drives the inflammatory state observed in CD36KO mice.

Endothelial Cell–specific CD36 Deletion Associates With Inflammation and Neutrophil Infiltration

The CD36KO mice displayed reduced levels of $Ly6C^{low}$ monocytes, which patrol the endothelium and are important for maintaining endothelial integrity,[33] and our microarrays showed upregulation of leukocyte transendothelial migration (Figure 1*A*). We next investigated whether loss of endothelial CD36 (EC-CD36KO) would recapitulate the phenotype observed in the intestines of CD36KO mice. CD36 floxed mice were crossed to C57BL6 mice expressing Cre driven by the Tie2 promoter, and validation of the EC-CD36KO mouse model is shown in Figure 7. The small intestine of EC-CD36KO mice exhibited increased fibronectin mRNA as compared with that of floxed controls ($P = .024$) (Figure 8*A*), but expression of collagen 1α or of α-SMA was not increased (Figure 8*A*) as observed in germline CD36KO mice. Among inflammation markers, there was upregulation of IL6 ($P = .04$), JNK 1 ($P = .05$), JNK 2 ($P = .02$), and p-JNK (Figure 8*B* and *C*) in the proximal intestine of EC-CD36KO mice as compared with controls. The mRNA expression of TNF-α and IL10 did not differ, whereas that of IL22 was

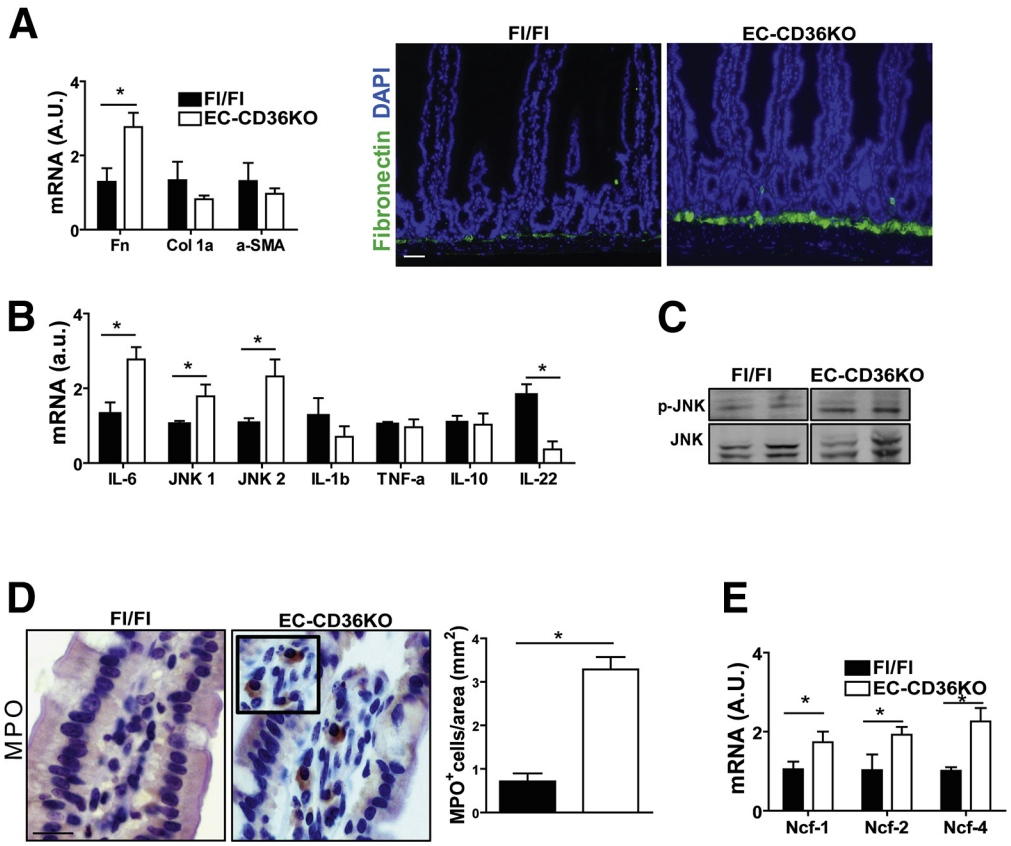

Figure 8. CD36 deletion in endothelial cells causes fibronectin accumulation, neutrophil infiltration, and IL6 upregulation in the small intestine. (*A*) Intestines of EC-CD36KO mice have increased level of fibronectin (qRT-PCR) as compared with those of floxed (Fl/Fl) controls ($P = .024$), but expression of col1α or of α-SMA is not increased. Increased level of fibronectin in EC-CD36KO mice documented by fluorescent staining (*right panel*); scale bar: 100 μm (data representative of 2 experiments). (*B*) Inflammation markers: proximal intestines of EC-CD36KO mice show increases in IL6 ($P = .04$), JNK 1 ($P = .05$), JNK 2 ($P = .02$), and p-JNK (*B* and *C*) as compared with controls. Expression of TNF-α and IL10 is unaltered, whereas that of IL22 is reduced ($P = .041$) (n = 8/genotype). (*D*) Intestines of EC-CD36KO mice show enhanced MPO staining as compared with Fl/Fl controls ($P = .01$) (representative of 2 experiments) and (*E*) increased mRNA levels for neutrophil proteins Ncf-1 ($P = .05$), Ncf-2 ($P = .041$), and Ncf-4 ($P = .009$) (n = 8/genotype). Scale bar: 30 μm. Graphs show mean ± SEM.

reduced ($P = .041$) (Figure 8*B*). Intestines of EC-CD36KO mice showed significant neutrophil infiltration as compared with Fl/Fl controls, which was evident from increased MPO staining (Figure 8*D*) and higher mRNA levels of Ncf-1 ($P = .05$), Ncf-2 ($P = .041$), and Ncf-4 ($P = .009$) (Figure 8*E*). Intestine permeability was also increased in EC-CD36KO mice (Figure 9*A*). Serum FITC-dextran levels in EC-CD36KO mice with or without a triolein challenge were increased at 2 hours ($P = .035$; $P_{\text{triolein}} = .41$) and 4 hours ($P = .05$; $P_{\text{triolein}} = .048$) as compared with floxed controls (Figure 9*A*). Intestinal permeability in EC-CD36KO mice challenged with triolein continued to be increased at 6 hours ($P = .043$). Consistent with this, serum endotoxin was higher in EC-CD36KO mice after 4 hours of a triolein bolus as compared with the floxed control group ($P = .05$) (Figure 9*B*). Two-photon microscopy was used to ascertain that the permeability increase was at the level of the intestinal epithelium. Leakage of luminal dextran (10 kDa) across the epithelium was evident in proximal intestines of EC-CD36KO mice, whereas no leakage was observed in the Fl/Fl controls ($P < .01$). Electron microscopy showed that similar to the small intestinal epithelium of germline CD36KO mice, desmosomes were shorter in EC-CD36KO mice ($P < .01$) (Figure 9*D*), and expression levels of desmocollin 2 mRNA were lower ($P = .05$) (Figure 9*E*). Also as in germline CD36KO, occludin protein levels were reduced in intestine of EC-CD36KO mice compared with Fl/Fl controls ($P = .042$) (Figure 9*F*). These data show that endothelial CD36 deletion disrupts intestinal homeostasis and causes neutrophil infiltration and epithelial barrier leakage, recapitulating notable abnormalities identified in germline CD36KO mice.

Discussion

The central findings of this study suggest that CD36 plays a critical and unsuspected role in maintenance of ECM remodeling and barrier integrity in the small intestine. Among the hallmarks of the CD36KO mouse are the presence of gut leakiness with accumulation of infiltrating

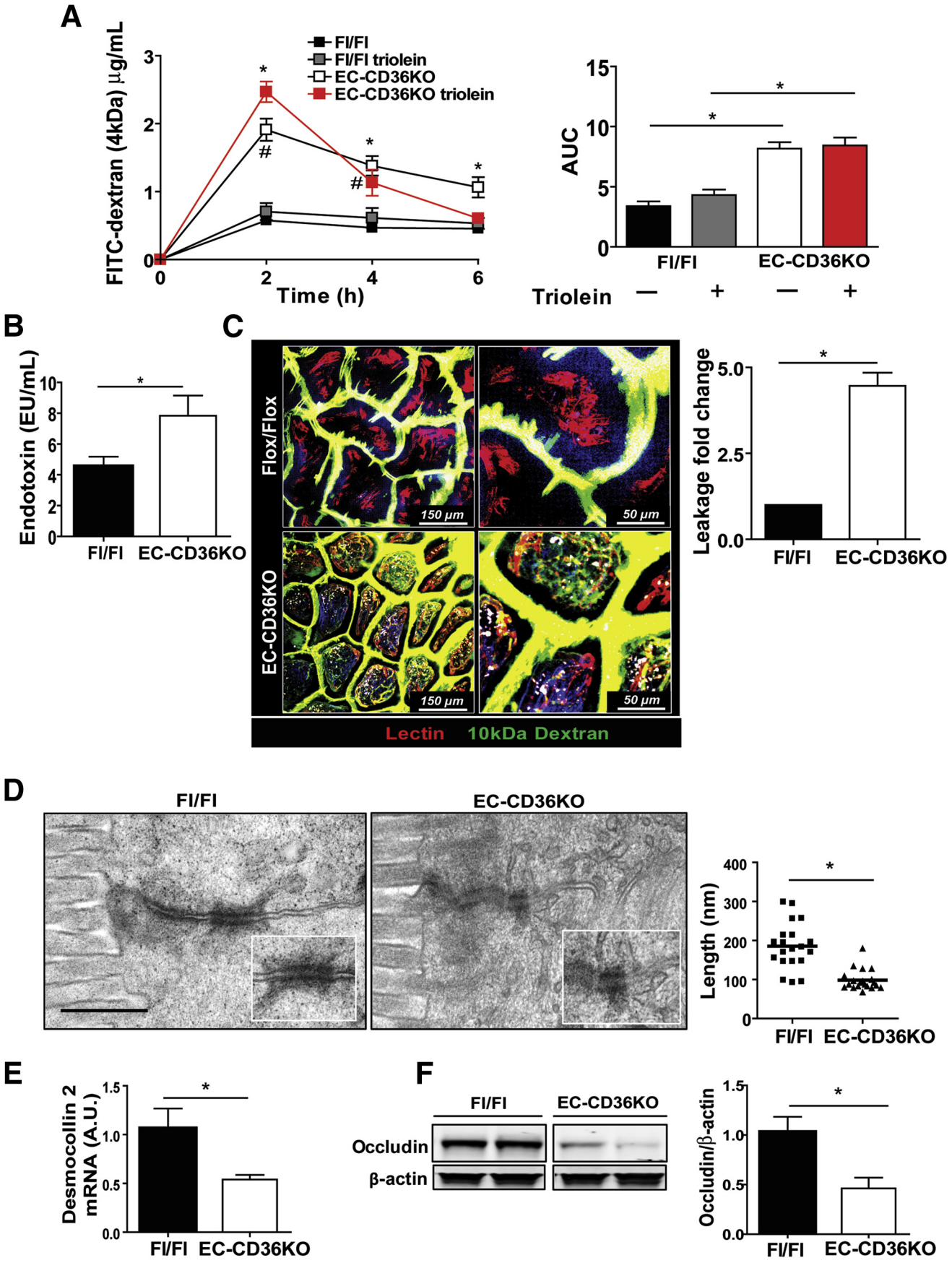
A
FITC-dextran (4kDa) μg/mL
Time (h)
Fl/Fl
Fl/Fl triolein
EC-CD36KO
EC-CD36KO triolein
AUC
Triolein
B
Endotoxin (EU/mL)
C
Flox/Flox
EC-CD36KO
150 μm
50 μm
Lectin 10kDa Dextran
Leakage fold change
D
Fl/Fl
EC-CD36KO
Length (nm)
E
Desmocollin 2 mRNA (A.U.)
F
Occludin
β-actin
Occludin/β-actin

neutrophils, systemic subclinical inflammation, and loss of the anti-inflammatory patrolling Ly6C^{low} monocytes. Although at first glance our data would appear to conflict with the well-established proinflammatory actions of CD36,[9,35] the findings are consistent with the versatile responses mediated by this receptor,[1,36] which, depending on the context, can promote or impair tissue homeostasis. There is extensive evidence to support contribution of CD36 in the inflammatory response, and targeting the protein has been proposed in a number of settings including atherosclerosis, cardiomyopathy, and fatty liver.[37,38] However, there is also evidence to support a role of CD36 in anti-inflammation or inflammation resolution. CD36 deletion impairs macrophage conversion to the alternatively activated, anti-inflammatory M2 phenotype, which requires CD36 lipid provision to lysosomes.[11] On monocytes/macrophages, CD36 facilitates phagocytosis of apoptotic neutrophils, allowing tissue healing,[10] and is important for maintaining the Ly6^{low} monocytes (Figure 5*C*), which function as endothelial housekeepers.[31,33,39]

Our bone marrow transplant data (Figure 6) indicate that non-hematopoietic cells are responsible for the systemic inflammation observed in CD36KO mice, and our findings with mice models support a major role for endothelial CD36 loss. Deletion of CD36 in endothelial cells recapitulates many aspects of the abnormal gut phenotype of germline CD36KO mice and is consistent with the altered endothelium promoting leukocyte migration into the gut (Figure 1*A*). Fibronectin accumulation and production of IL6 (Figure 8) are early signs of endothelial inflammation. In particular, fibronectin accumulation regulates activation of mediators such as nuclear factor kappa B,[40,41] an established inducer of cytokines including IL6.

IL6 promotes neutrophil recruitment and plays an important role in regulating the gut barrier.[42,43] IL6 level is increased in serum and tissues of patients with Crohn's disease, and high IL6 has been implicated in etiology of experimental colitis in mice.[44,45] IL6 increases barrier permeability by activating the JNK pathway and enhancing expression of the TJ protein claudin-2.[46,47] We did not detect changes in claudin-2 expression despite JNK activation in intestines of mice with either global or endothelial CD36 deficiency (data not shown). In addition to transcriptional regulation, claudin-2 is subject to extensive posttranslational modification (phosphorylation by multiple kinases and SUMOylation), but the potential regulatory effects of these modifications remain poorly understood[48] and were not explored in this study.

In contrast to the increase in IL6, the level of IL22, a member of the IL10-related cytokine family, was markedly reduced in intestines of germline CD36KO and EC-CD36KO mice. IL22 protects the mucosal barrier against pathogens and promotes tissue healing.[49,50] Administration of IL22 to obese mice was shown to reduce endotoxemia and chronic inflammation.[51] The lower level of IL22 together with the higher level of IL6 in the intestines of germline CD36KO and EC-CD36KO mice likely drive the disruption of barrier integrity and chronic inflammation observed in these mice.

Transepithelial migration of neutrophils associates with disruption of barrier function and correlates with disease flares and severity in inflammatory bowel disease.[7,24] The first intercellular adhesion complex encountered by migrating neutrophils would be the desmosomes, and reduction of desmocollin 2 expression correlated with altered epithelial barrier function in inflammatory bowel disease.[52] We observed shortening of desmosomes with lower expression of desmocollin 2 in both CD36KO and EC-CD36KO mice (Figures 2 and 9), but whether this plays an important role in the increase in intestinal permeability remains unclear. We also report a decreased level of the tight junction protein occludin in CD36KO and EC-CD36KO mice models. Occludin inhibits transepithelial neutrophil migration,[53] and its level was shown to be reduced in inflammatory bowel disease.[54] However, occludin deletion in mice did not alter gut permeability,[55] and understanding its contribution to the intestinal phenotype of CD36KO and EC-CD36KO mice will require further study. In contrast to endothelial cell CD36 deletion, enterocyte CD36 deletion did not cause gut neutrophil infiltration or altered intestinal

Figure 9. (***See previous page***). **Epithelial barrier permeability is compromised in mice with CD36 deletion specific to endothelial cells.** (*A*) Plasma levels of FITC-dextran (4 kDa) at 0, 2, 4, and 6 hours after its intragastric administration to Flox/Flox (Fl/Fl) and EC-CD36KO mice (n = 6/genotype). A week later, the same mice groups received bolus of triolein (4.5 μL/g body weight) 30 minutes before FITC-dextran. Intestinal permeability is increased in all EC-CD36KO mice at 2 hours ($P = .035$; $P_{triolein} = .041$) and 4 hours ($P = .05$; $P_{triolein} = .048$) and only in EC-CD36KO given triolein at 6 hours ($P = .43$). $^{\#}$Fl/Fl versus EC-CD36KO, *Fl/Fl$_{triolein}$ versus EC-CD36KO$_{triolein}$. *Right panel* shows area under the curve (AUC) for FITC-dextran assay; AUCs for EC-CD36KO and EC-CD36KO$_{triolein}$ are increased compared with appropriate Fl/Fl controls ($P < .001$ and $P = .002$, respectively). (*B*) Higher endotoxin levels in plasma of EC-CD36KO as compared with Fl/Fl mice at 4 hours after triolein bolus, $P = .05$ (n = 4/genotype). (*C*) Two-photon optical images showing epithelial leakage of fluorescein-dextran in EC-CD36KO mice ($P < .01$) compared with floxed control mice. Fluorescein-dextran 10 kDa (*green*) was injected intraluminally into anesthetized mice, and DyLight 594–conjugated tomato lectin (*red*) was given by retro-orbital injection 10 minutes before imaging from the luminal side (n = 3 mice/genotype). Quantification of leakage is expressed as fold change of FITC-dextran fluorescence inside the villus versus fluorescence between epithelial cells measured in 5 random villi/mouse. (*D*) Electron microscopy showing reduced length of desmosomes in EC-CD36KO mice compared with Fl/Fl controls ($P < .001$). (*E*) Desmocollin 2 expression is decreased in proximal intestines of EC-CD36KO (n = 4/genotype) ($P = .05$). (*F*) Immunoblots of occludin in lysates of proximal intestines showing reduced levels in EC-CD36KO mice. Graph shows densitometry of occludin/β-actin compared with that of Fl/Fl controls ($P = .042$) (representative of 2 experiments). (*A–E*) representative of 3 experiments. All graphs show means ± SEM.

permeability, but the role of enterocyte CD36 cannot be ruled out without additional studies under different inflammatory challenges.

Finally, CD36 has pleiotropic functions that involve native immunity and lipid metabolism, and factors we did not consider in this study could alter intestinal permeability. For example, the gut microbiota that can shape the intestinal environment driving homeostasis or inflammation[56] might be impacted by CD36 deficiency. In addition, alterations in hepatic metabolism and inflammation could influence gut barrier permeability.[57] How CD36 deletion affects the crosstalk between intestinal cells and microbiota as well as the gut-liver axis is unknown.

Our findings in mice might be relevant to humans. CD36 deficiency has a relatively high frequency in populations of African and Asian ancestry, and single nucleotide polymorphisms that reduce CD36 level are relatively common.[58] Carriers of the minor allele (G) of coding single nucleotide polymorphism rs3211938 (~20% of African Americans) have ~50% reduction of CD36 expression, and this associates with increased endothelial stiffness and with an altered nitric oxide–cyclic guanosine monophosphate pathway.[59] Our preliminary data show increased blood levels of activated neutrophils in these subjects, suggesting presence of subclinical inflammation (data not shown). Reduction of CD36 gene expression was reported in the ileum and colon of subjects with inflammatory bowel disease by array analysis.[60]

In conclusion, our findings suggest that the inflamed endothelium, in this case a result of CD36 loss, plays an important role in promoting neutrophil recruitment impairing epithelial barrier integrity at the level of the small intestine. The role of endothelial dysfunction in gut inflammatory diseases warrants further investigation.

References

1. Silverstein RL, Febbraio M. CD36, a scavenger receptor involved in immunity, metabolism, angiogenesis, and behavior. Sci Signal 2009;2:re3.
2. Abumrad NA, Davidson NO. Role of the gut in lipid homeostasis. Physiol Rev 2012;92:1061–1085.
3. Drover VA, Ajmal M, Nassir F, et al. CD36 deficiency impairs intestinal lipid secretion and clearance of chylomicrons from the blood. J Clin Invest 2005;115:1290–1297.
4. Nauli AM, Nassir F, Zheng S, et al. CD36 is important for chylomicron formation and secretion and may mediate cholesterol uptake in the proximal intestine. Gastroenterology 2006;131:1197–1207.
5. Peterson LW, Artis D. Intestinal epithelial cells: regulators of barrier function and immune homeostasis. Nat Rev Immunol 2014;14:141–153.
6. Leoni G, Neumann PA, Sumagin R, et al. Wound repair: role of immune-epithelial interactions. Mucosal Immunol 2015;8:959–968.
7. Parkos CA. Neutrophil-epithelial interactions: a double-edged sword. Am J Pathol 2016;186:1404–1416.
8. Stuart LM, Deng J, Silver JM, et al. Response to Staphylococcus aureus requires CD36-mediated phagocytosis triggered by the COOH-terminal cytoplasmic domain. J Cell Biol 2005;170:477–485.
9. Stewart CR, Stuart LM, Wilkinson K, et al. CD36 ligands promote sterile inflammation through assembly of a Toll-like receptor 4 and 6 heterodimer. Nat Immunol 2010;11:155–161.
10. Ballesteros I, Cuartero MI, Pradillo JM, et al. Rosiglitazone-induced CD36 up-regulation resolves inflammation by PPARgamma and 5-LO-dependent pathways. J Leukoc Biol 2014;95:587–598.
11. Huang SC, Everts B, Ivanova Y, et al. Cell-intrinsic lysosomal lipolysis is essential for alternative activation of macrophages. Nat Immunol 2014;15:846–855.
12. Oh J, Riek AE, Weng S, et al. Endoplasmic reticulum stress controls M2 macrophage differentiation and foam cell formation. J Biol Chem 2012;287:11629–11641.
13. Asch AS, Liu I, Briccetti FM, et al. Analysis of CD36 binding domains: ligand specificity controlled by dephosphorylation of an ectodomain. Science 1993;262:1436–1440.
14. Lawler PR, Lawler J. Molecular basis for the regulation of angiogenesis by thrombospondin-1 and -2. Cold Spring Harb Perspect Med 2012;2:a006627.
15. Sorokin L. The impact of the extracellular matrix on inflammation. Nat Rev Immunol 2010;10:712–723.
16. Hallmann R, Zhang X, Di Russo J, et al. The regulation of immune cell trafficking by the extracellular matrix. Curr Opin Cell Biol 2015;36:54–61.
17. Shimshoni E, Yablecovitch D, Baram L, et al. ECM remodelling in IBD: innocent bystander or partner in crime? the emerging role of extracellular molecular events in sustaining intestinal inflammation. Gut 2015;64:367–372.
18. Gautier EL, Westerterp M, Bhagwat N, et al. HDL and Glut1 inhibition reverse a hypermetabolic state in mouse models of myeloproliferative disorders. J Exp Med 2013;210:339–353.
19. McDole JR, Wheeler LW, McDonald KG, et al. Goblet cells deliver luminal antigen to CD103+ dendritic cells in the small intestine. Nature 2012;483:345–349.
20. Yona S, Kim KW, Wolf Y, et al. Fate mapping reveals origins and dynamics of monocytes and tissue macrophages under homeostasis. Immunity 2013;38:79–91.
21. Yoshino J, Mills KF, Yoon MJ, et al. Nicotinamide mononucleotide, a key NAD(+) intermediate, treats the pathophysiology of diet- and age-induced diabetes in mice. Cell Metab 2011;14:528–536.
22. Tran TT, Poirier H, Clement L, et al. Luminal lipid regulates CD36 levels and downstream signaling to stimulate chylomicron synthesis. J Biol Chem 2011;286:25201–25210.
23. Ji Y, Sakata Y, Yang Q, et al. Activation of rat intestinal mucosal mast cells by fat absorption. Am J Physiol Gastrointest Liver Physiol 2012;302:G1292–G1300.
24. Nash S, Stafford J, Madara JL. Effects of polymorphonuclear leukocyte transmigration on the barrier function of cultured intestinal epithelial monolayers. J Clin Invest 1987;80:1104–1113.
25. Holmes JL, Van Itallie CM, Rasmussen JE, et al. Claudin profiling in the mouse during postnatal intestinal

development and along the gastrointestinal tract reveals complex expression patterns. Gene Expr Patterns 2006; 6:581–588.
26. Groschwitz KR, Hogan SP. Intestinal barrier function: molecular regulation and disease pathogenesis. J Allergy Clin Immunol 2009;124:3–20; quiz 21–22.
27. Ohman L, Tornblom H, Simren M. Crosstalk at the mucosal border: importance of the gut microenvironment in IBS. Nat Rev Gastroenterol Hepatol 2015;12:36–49.
28. Fournier BM, Parkos CA. The role of neutrophils during intestinal inflammation. Mucosal Immunol 2012;5:354–366.
29. Jakubzick C, Gautier EL, Gibbings SL, et al. Minimal differentiation of classical monocytes as they survey steady-state tissues and transport antigen to lymph nodes. Immunity 2013;39:599–610.
30. Ingersoll MA, Platt AM, Potteaux S, et al. Monocyte trafficking in acute and chronic inflammation. Trends Immunol 2011;32:470–477.
31. Shi C, Pamer EG. Monocyte recruitment during infection and inflammation. Nat Rev Immunol 2011;11:762–774.
32. Pellicoro A, Ramachandran P, Iredale JP, et al. Liver fibrosis and repair: immune regulation of wound healing in a solid organ. Nat Rev Immunol 2014;14:181–194.
33. Auffray C, Fogg D, Garfa M, et al. Monitoring of blood vessels and tissues by a population of monocytes with patrolling behavior. Science 2007;317:666–670.
34. Won WJ, Bachmann MF, Kearney JF. CD36 is differentially expressed on B cell subsets during development and in responses to antigen. J Immunol 2008; 180:230–237.
35. Silverstein RL. Inflammation, atherosclerosis, and arterial thrombosis: role of the scavenger receptor CD36. Cleve Clin J Med 2009;76(Suppl 2):S27–S30.
36. Canton J, Neculai D, Grinstein S. Scavenger receptors in homeostasis and immunity. Nat Rev Immunol 2013; 13:621–634.
37. Park YM. CD36, a scavenger receptor implicated in atherosclerosis. Exp Mol Med 2014;46:e99.
38. Steneberg P, Sykaras AG, Backlund F, et al. Hyperinsulinemia enhances hepatic expression of the fatty acid transporter Cd36 and provokes hepatosteatosis and hepatic insulin resistance. J Biol Chem 2015; 290:19034–19043.
39. Thomas G, Tacke R, Hedrick CC, et al. Nonclassical patrolling monocyte function in the vasculature. Arterioscler Thromb Vasc Biol 2015;35:1306–1316.
40. Orr AW, Sanders JM, Bevard M, et al. The subendothelial extracellular matrix modulates NF-kappaB activation by flow: a potential role in atherosclerosis. J Cell Biol 2005; 169:191–202.
41. Baeyens N, Bandyopadhyay C, Coon BG, et al. Endothelial fluid shear stress sensing in vascular health and disease. J Clin Invest 2016;126:821–828.
42. Scheller J, Chalaris A, Schmidt-Arras D, et al. The pro- and anti-inflammatory properties of the cytokine interleukin-6. Biochim Biophys Acta 2011;1813:878–888.
43. Man AL, Bertelli E, Rentini S, et al. Age-associated modifications of intestinal permeability and innate immunity in human small intestine. Clin Sci (Lond) 2015; 129:515–527.
44. Atreya R, Mudter J, Finotto S, et al. Blockade of interleukin 6 trans signaling suppresses T-cell resistance against apoptosis in chronic intestinal inflammation: evidence in crohn disease and experimental colitis in vivo. Nat Med 2000;6:583–588.
45. Yamamoto M, Yoshizaki K, Kishimoto T, et al. IL-6 is required for the development of Th1 cell-mediated murine colitis. J Immunol 2000;164:4878–4882.
46. Suzuki T, Yoshinaga N, Tanabe S. Interleukin-6 (IL-6) regulates claudin-2 expression and tight junction permeability in intestinal epithelium. J Biol Chem 2011; 286:31263–31271.
47. Al-Sadi R, Ye D, Boivin M, et al. Interleukin-6 modulation of intestinal epithelial tight junction permeability is mediated by JNK pathway activation of claudin-2 gene. PLoS One 2014;9:e85345.
48. González-Marisca L, Garay E, Quirós M. Regulation of claudins by posttranslational modifications and cell-signaling cascades. Current Topics in Membranes 2010;65:113–150.
49. Colonna M. Interleukin-22-producing natural killer cells and lymphoid tissue inducer-like cells in mucosal immunity. Immunity 2009;31:15–23.
50. Ouyang W, Rutz S, Crellin NK, et al. Regulation and functions of the IL-10 family of cytokines in inflammation and disease. Annu Rev Immunol 2011;29:71–109.
51. Wang X, Ota N, Manzanillo P, et al. Interleukin-22 alleviates metabolic disorders and restores mucosal immunity in diabetes. Nature 2014;514:237–241.
52. Gassler N, Rohr C, Schneider A, et al. Inflammatory bowel disease is associated with changes of enterocytic junctions. Am J Physiol Gastrointest Liver Physiol 2001; 281:G216–G228.
53. Huber D, Balda MS, Matter K. Occludin modulates transepithelial migration of neutrophils. J Biol Chem 2000;275:5773–5778.
54. Kucharzik T, Walsh SV, Chen J, et al. Neutrophil transmigration in inflammatory bowel disease is associated with differential expression of epithelial intercellular junction proteins. Am J Pathol 2001;159:2001–2009.
55. Saitou M, Furuse M, Sasaki H, et al. Complex phenotype of mice lacking occludin, a component of tight junction strands. Mol Biol Cell 2000;11:4131–4142.
56. Ohland CL, Jobin C. Microbial activities and intestinal homeostasis: a delicate balance between health and disease. Cell Mol Gastroenterol Hepatol 2015; 1:28–40.
57. Luther J, Garber JJ, Khalili H, et al. Hepatic injury in nonalcoholic steatohepatitis contributes to altered intestinal permeability. Cell Mol Gastroenterol Hepatol 2015;1:222–232.
58. Love-Gregory L, Sherva R, Schappe T, et al. Common CD36 SNPs reduce protein expression and may contribute to a protective atherogenic profile. Hum Mol Genet 2011;20:193–201.
59. Shibao CA, Celedonio JE, Ramirez CE, et al. A common CD36 variant influences endothelial function and response to treatment with phosphodiesterase 5 inhibition. J Clin Endocrinol Metab 2016; 101:2751–2758.

60. Heimerl S, Moehle C, Zahn A, et al. Alterations in intestinal fatty acid metabolism in inflammatory bowel disease. Biochim Biophys Acta 2006;1762:341–350.

Received December 21, 2015. Accepted September 8, 2016.

Reprint requests
Address requests for reprints to: Nada A. Abumrad, PhD, or Vincenza Cifarelli, PhD, Department of Medicine, Center for Human Nutrition, Washington University School of Medicine, Campus Box 8031, St. Louis, Missouri 63110. e-mail: nabumrad@wustl.edu or cifarelli@wustl.edu; fax: (314) 362-8230.

Current address for Stoyan Ivanov: Institut National de la Santé et de la Recherche Médicale (INSERM) U1065, Centre Méditerranéen de Médecine Moléculaire, Nice, France.

Conflicts of interest
The authors disclose no conflicts.

Funding
Supported by National Institutes of Health grants R01 DK033301 and R01 DK060022 (N.A.A.); T32HL007275 (V.C.); R01 AI049653 and R21 AG046743 (G.J.R.); HL38180, DK56260, and Digestive Disease Research Core Center DK52574 (N.O.D.), HL45095 and HL73029 (I.J.G.); and by the Nutrition and Obesity Research Center supported by P30-DK-056341.